



Novel Pd(II) and Pt(II) complexes of N,N-donor benzimidazole ligand: Synthesis, spectral, electrochemical, DFT studies and evaluation of biological activity

Nour T. Abdel Ghani, Ahmed M. Mansour*

Chemistry Department, Faculty of Science, Cairo University, Gamaa Street, Giza 12613, Egypt

ARTICLE INFO

Article history:

Received 3 November 2010

Received in revised form 7 March 2011

Accepted 20 April 2011

Available online 27 April 2011

Keywords:

Benzimidazole

Platinum complex

DFT

NBO

Antitumor

ABSTRACT

(1H-benzimidazol-2-ylmethyl)-(4-nitro-phenyl)-amine (L) and its Pd(II) and Pt(II) complexes have been synthesized as potential anticancer compounds and their structures were elucidated using a variety of physico-chemical techniques. The activation thermodynamic parameters were calculated using non-isothermal methods. Theoretical calculations invoking geometry optimization, charge distribution and molecular orbital description HOMO and LUMO were done using density functional theory. Natural bond orbital analysis (NBO) was performed for the investigation of major stabilizing orbital interactions. The experimental results, and the calculated molecular parameters, bond distances and angles, revealed a square-planar geometry around the metallic center through the pyridine-type nitrogen of the benzimidazole ring (N_{py}) and secondary amino group (NH_{sec}) and two chlorine atoms. Electrochemical investigation of the complexes showed some irreversible, reversible, and quasi-reversible redox reactions. The synthesized ligand, in comparison to its metal complexes was screened for its antibacterial activity. The cytotoxicity assay of the complexes against three-cell lines *breast cancer* (MCF7), *colon Carcinoma* (HCT) and *human hepatocellular Carcinoma* (Hep-G2) was studied.

© 2011 Elsevier B.V. All rights reserved.

1. Introduction

Despite the widespread use of cis-diaminedichloroplatinum(II) (cis-platin) as an anticancer drug there is still scope for improvement, with respect to reduced toxicity [1], increased clinical effectiveness, broader spectrum of action, elimination of side effects (e.g. nausea, hearing loss, vomiting, etc.), increased solubility, and the ability to use it in combination with other drugs. Many derivatives of cis-platin also inhibit growth, and these compounds have at least one N–H group [2] (one of the reasons for choosing the ligand under study), which is responsible for important hydrogen-bond donor properties, either in the approach of the biological target or the final structure. Recently, interest was carried out in the developing cis-platin analogs, which have heterocyclic amine ligands coordinated to the cytotoxic platinum(II) moiety. Several platinum complexes with N-heterocyclic ligands such as imidazole, thiazole, benzimidazole, benzothiazole, and benzoxazole were reported [3]. The benzimidazole scaffold is a useful structural motif for displaying chemical functionality in biologically active molecules. Some of its derivatives have potent biological activities as antitumor [4], anti-HIV [5], anti-Parkinson [6], and antimicrobial [7] agents. At the same time, because of the coordination chemistry of azoles acting as ligands in transition metal compounds, the che-

lating ligands incorporating benzimidazole groups have been extensively studied in the context of modeling biological systems in recent years [8]. Our aim was to take into account all the previously mentioned properties of anticancer drugs and synthesize new platinum(II) and palladium(II) complexes of new N,N donor benzimidazole derivatived cis-platin analogs that could prove to be potent antitumor agents through characterization and elucidation of their structures using different spectroscopic, thermal and conductance measurements. Density functional theory (DFT) calculations were done in order to correlate between the theoretical and experimental results.

2. Experimental

2.1. Synthesis of ligand (L) and its complexes

The benzimidazole L (Fig. 1) was prepared by condensation of equimolar quantities of 2-chloromethylbenzimidazole [9] with 4-nitroaniline. The reaction mixture was refluxed in ethanol in the presence of sodium iodide for about 18–24 h. Then, the reaction mixture was neutralized and the solid was separated by dilution with de-ionized water, and recrystallized from ethanol.

One millimole K_2PdCl_4 was prepared by dissolving 0.177 g $PdCl_2$ in 0.149 g/50 ml aqueous potassium chloride solution. The solid metal complexes of the benzimidazole compound (L) with Pd(II), and Pt(II) metal ions were prepared by adding a hot ethanolic

* Corresponding author. Fax: +20 2 35728843.

E-mail address: inorganic_am@yahoo.com (A.M. Mansour).

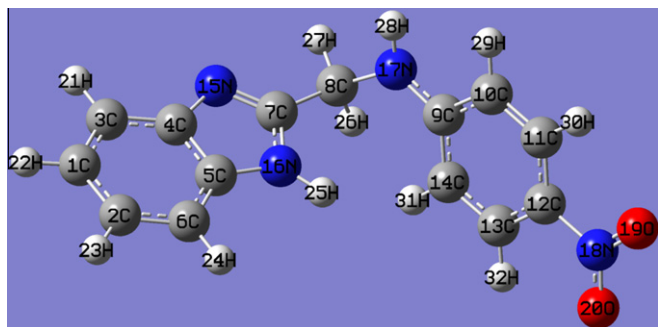


Fig. 1. The optimized structure of benzimidazole L.

solution (60 °C) of the ligand (1 mmol) to a hot aqueous solution (60 °C) of the metal ions (1 mmol; K_2PdCl_4 , or K_2PtCl_4). The resulting mixtures were stirred under reflux for about 1–2 h, whereupon the complexes precipitated.

2.2. Instruments

Infrared spectra of the ligand and its complexes were recorded in potassium bromide discs using *FTIR-460 plus*, JASCO, Japan, in 4000–200 cm^{-1} region. The 1H NMR spectra were run at 300 MHz using dimethylsulfoxide ($DMSO-d_6$) as a solvent and tetramethylsilane (TMS) as a reference using *Varian-Oxford Mercury VX-300 NMR*. Deuterium oxide (D_2O) was used to confirm the presence of ionizable protons. The mass spectra measurements were recorded with the aid of a *SHIMADZU QP-2010 plus* mass spectrometer at 70 eV. The thermogravimetric analysis (TGA) and differential thermal analysis (DTA) were carried out in dynamic nitrogen atmosphere (20 $ml\ min^{-1}$) with a heating rate of 10 °C min^{-1} using *DTG-60H SIMULTANEOUS DTA-TG APPARATUS-SHIMADZU*. Digital *Jenway 4330* Conductivity-pH meter with (1.02) cell constant was used for pH and molar conductance measurements. Spectrophotometric measurements were carried out using automated spectrophotometer UV-Vis. *SHIMADZU Lambda 4B* using 1 cm matched quartz cells. Cyclic voltammetry measurements were performed using a three-electrode configuration cell connected to an EG and G scanning potentiostat model 372. A Pt disc was used as working electrode and a Pt wire as auxiliary electrode. The reference electrode was Ag/AgCl electrode adjusted to 0.00 V versus SCE. Sample solutions (50 ml) of 10^{-3} M concentration in DMF with 0.1 M $NaClO_4 \cdot H_2O$ as supporting electrolyte were used for the measurements. A potential range of +2000 to –2000 mV, with a scan rate of 100 $mV\ s^{-1}$ was used.

2.3. Theoretical calculations

The molecular structure of the benzimidazole L in the ground state was optimized by a DFT method using B3LYP functional [10,11] combined with 6-311G(d,p) and LANL2DZ basis sets. Calculations were carried out using GAUSSIAN 03 [12]. The vibrational frequencies of the benzimidazole (L) and the corresponding normal modes were evaluated at the optimized geometry [13] using the same basis sets. Vibrational modes were analyzed using GAUSSVIEW software [14]. The main reason for choosing the LANL2DZ basis set is its inclusion of relativistic effect that is essential for heavy elements, e.g. Pd(II) and Pt(II), in order to compare between the optimized structures of the ligand and its complexes. The 1H NMR chemical shifts of the benzimidazole (L) were computed at the B3LYP/6-311+G(2d,p) level of theory in the gaseous state by applying the (GIAO) approach [15] and the values for the 1H -isotro-

pic were referenced to TMS, which was calculated at the same level of theory ($\delta_{TMS} = 31.88$). The optimized structures, vibrational frequencies, 1H chemical shifts, and the natural bond (NBO) analysis of the metal complexes were obtained at B3LYP/LANL2DZ level of theory.

2.4. Biological activity

2.4.1. Antimicrobial activity

The antimicrobial activities of the test samples were determined using a modified Kirby–Bauer disc diffusion method [16] under standard conditions using *Mueller–Hinton* agar medium, as described by NCCLS [17]. The antimicrobial activities were carried out using culture of *Bacillus subtilis*, *Staphylococcus aureus*, *Streptococcus faecalis* as Gram-positive bacteria and *Escherichia coli*, *Pseudomonas aeruginosa*, *Neisseria gonorrhoeae* as Gram-negative bacteria. Briefly, 100 μl of the test bacteria were grown in 10 ml of fresh media until they reached a count of approximately 108 cells/ml. 100 μl of microbial suspension was spread onto agar plates corresponding to the broth in which they were maintained. DMSO (0.1 ml) alone was used as control under the same conditions for each microorganism, subtracting the diameter of inhibition zone resulting with DMSO, from that obtained in each case. The results were compared with a similar run of *Tetracycline* as an antibacterial. The antimicrobial activities could be calculated as a mean of three replicates.

2.4.2. Cell culture and cytotoxicity determination

Three human cancer cell lines were used for *in vitro* screening experiments; *breast cancer* (MCF7), *colon Carcinoma* (HCT) and *human hepatocellular Carcinoma* (Hep-G2). They were obtained frozen in liquid nitrogen (–180 °C) from the American Type Culture Collection. The tumor cell lines were maintained in the National Cancer Institute, Cairo, Egypt, by serial sub-culturing. Cell culture cytotoxicity assays were carried out as described previously [18]. RPMI-1640 medium was used for culturing and maintenance of the human tumor cell lines [18]. Cells were seeded in 96-well plates at a concentration of 5×10^4 – 10^5 cell/well in a fresh medium and left to attach to the plates for 24 h. Growth inhibition of cells was calculated spectrophotometrically using a standard method with the protein-binding dye sulforhodamine B (SRB) [19]. The results were compared with a similar run of *cis-platin* as an antitumor compound.

3. Result and discussion

3.1. IR spectral studies

The theoretical IR spectra of the benzimidazole L were obtained at DFT/B3LYP level of theory using 6-311G(d,p) and LANL2DZ basis sets. At this level of theory, the calculated harmonic force constants and frequencies are higher than the experimental values, due to basis set truncation and neglecting of electron correlation and mechanical anharmonicity [20]. To compensate these shortcomings, scale factors were introduced and an explanation of this approach was discussed [21]. Two different methods were applied: (i) *uniform scaling* [21], the scaling factors are 0.963 for 6-311G(d,p) and 0.970 for LANL2DZ basis sets; (ii) *linear regression method* [22], in this method, the plot of the calculated frequencies versus their experimental values resulted in a straight line, whose equation was used to correct the calculated frequencies (ν_{calc}).

The benzimidazole L has a strong intermolecular hydrogen bond [3] $N16-H \cdots N15$ [23], which makes the IR spectrum shows strong and broad absorption band in the region 3500–2200 cm^{-1} . However, the band located at 3360 cm^{-1} is assigned to the

benzimidazolic NH (NH_{Bz}), while its theoretical value is observed at 3497 cm^{-1} as calculated by 6-311G(d,p). This discrepancy may be justified on the basis that the calculation was performed on a single molecule in the gaseous state contrary to the experimental values that were recorded in presence of intermolecular interactions. In complexes, the $\nu(\text{NH}_{\text{Bz}})$ is observed at 3356 cm^{-1} (Pd-L) and 3355 cm^{-1} (Pt-L). This confirms that the NH_{Bz} group remains intact in the complexes [3,24].

The sharp band at 3479 cm^{-1} in the benzimidazole L is assigned to $\nu(\text{NH}_{\text{sec}})$ that is in a good agreement with the theoretical value (Supplementary material, Table S1). This band is still observed in its complexes, but it is shifted to lower frequencies and becomes broad at 3386 cm^{-1} (Pd-L) and 3418 cm^{-1} (Pt-L) indicating its involvement in the coordination sphere [25]. The band at 1631 cm^{-1} is assigned to $\nu(\text{C}=\text{N})$, which deviates from the unscaled vibration mode (1665 cm^{-1}) and the previously reported data [26] owing to the presence of intermolecular hydrogen bond. It was found that the scaling is not necessary in the latter range as previously reported [27]. In complexes, the $\nu(\text{C}=\text{N})$ is shifted to lower frequencies as compared with the free group resulting in its overlapping with $\nu(\text{C}=\text{C})$ in the same region and thus it is difficult to assign this vibration mode experimentally.

Unfortunately, the metal–nitrogen stretching bands could not be distinguished from other ring skeleton vibrations present in this region [3]. The far-IR spectrum of Pd-L complex shows two medium bands at 368 and 362 cm^{-1} due to $\nu(\text{Pd}-\text{Cl})$ in a cis-square planar structure [24]. Similarly, the platinum complex shows these modes at 372 and 360 cm^{-1} . The band at 850 cm^{-1} in the spectrum of the palladium complex is assigned to the rocking mode of the water of hydration [28]. Other vibration modes of the benzimidazole L are assigned (Supplementary material, Table S1). Finally, IR study reveals that the ligand coordinated to the metal ions via the pyridine-type nitrogen (N_{py}) of the benzimidazole ring and secondary amino group (NH_{sec}).

3.2. ^1H NMR studies

The NH_{Bz} signal appears at 12.39 ppm [29] in the benzimidazole L and moves downfield in its complexes; 13.36 ppm for Pd-L and 13.61 ppm for Pt-L complex. This shift is related to the charge density change in the benzimidazole ring, which supports the fact that the coordination occurs via the pyridine-type nitrogen. The triplet signal at 6.69 ppm in the free ligand is due to the NH_{sec} group that is obscured by the aromatic signals, whereas the doublet signal at 4.64 ppm is assigned to the CH_2 group. In complexes, both signals move downfield owing to the participation of the NH_{sec} group in the chelation (Supplementary material, Fig. S1). The methylene group appears as a pair of quartet at 5.14 and 5.52 ppm for Pd-L and 4.81 and 4.94 ppm for Pt-L, as the CH_2 protons are no longer isochronous, where the equatorial proton points away from the metal ion than the axial one does.

The protons of the aniline ring give rise to four-line pattern at 6.59 , 6.75 ppm for the two protons in the ortho-position with respect to NH_{sec} and 7.93 , 8.03 ppm with respect to the nitro group. However, the signals of the benzimidazole protons are much broader [30] and are shown at 7.14 , 7.15 , 7.49 , and 7.55 ppm . In complexes, the aromatic protons nearest the coordination centers are found to suffer maximum downfield shifts compared with the other aromatic protons.

The calculated chemical shifts of the methylene (4.69 ppm) and the NH_{sec} (6.52 ppm) groups in the benzimidazole (L), are in agreement with the experimental values. The theoretical chemical shifts at 8.03 , 7.93 , 6.75 , and 6.59 ppm in the benzimidazole L are assigned to the aromatic protons of the aniline moiety, while the signals at 7.55 , 7.49 , 7.15 , and 7.14 ppm are attributed to the benzimidazolic protons. Thus, the experimental values are slightly

smaller than the calculated ones. However, the experimental chemical shift of the NH_{Bz} proton is shifted towards higher magnetic field than the calculated one by 4.29 ppm , as previously reported [31]. This may be due to neglect of the non-specific solute–solvent interactions (in the gas phase), and the intermolecular hydrogen bond in our calculations as compared with the experimental chemical shifts that are obtained from the DMSO solutions (hydrogen-bonded solvent).

3.3. Mass spectrometry

The electron impact mass spectra of the ligand L and its complexes were recorded at 70 eV . The benzimidazole L has a strong molecular ion peak at m/z 268, and decomposes to offer a peak at m/z 131, which is assigned to 2-methylene benzimidazole. The fragment at m/z 118 is recognized to the benzimidazole ring, while that at m/z 93 is known to the aniline moiety. The mass spectrum of Pd-L complex has M^+ at m/z 481 corresponding to $[\text{PdLCl}_2 \cdot 2\text{H}_2\text{O}]^+$ with three fragmentation routes as shown in Scheme 1.

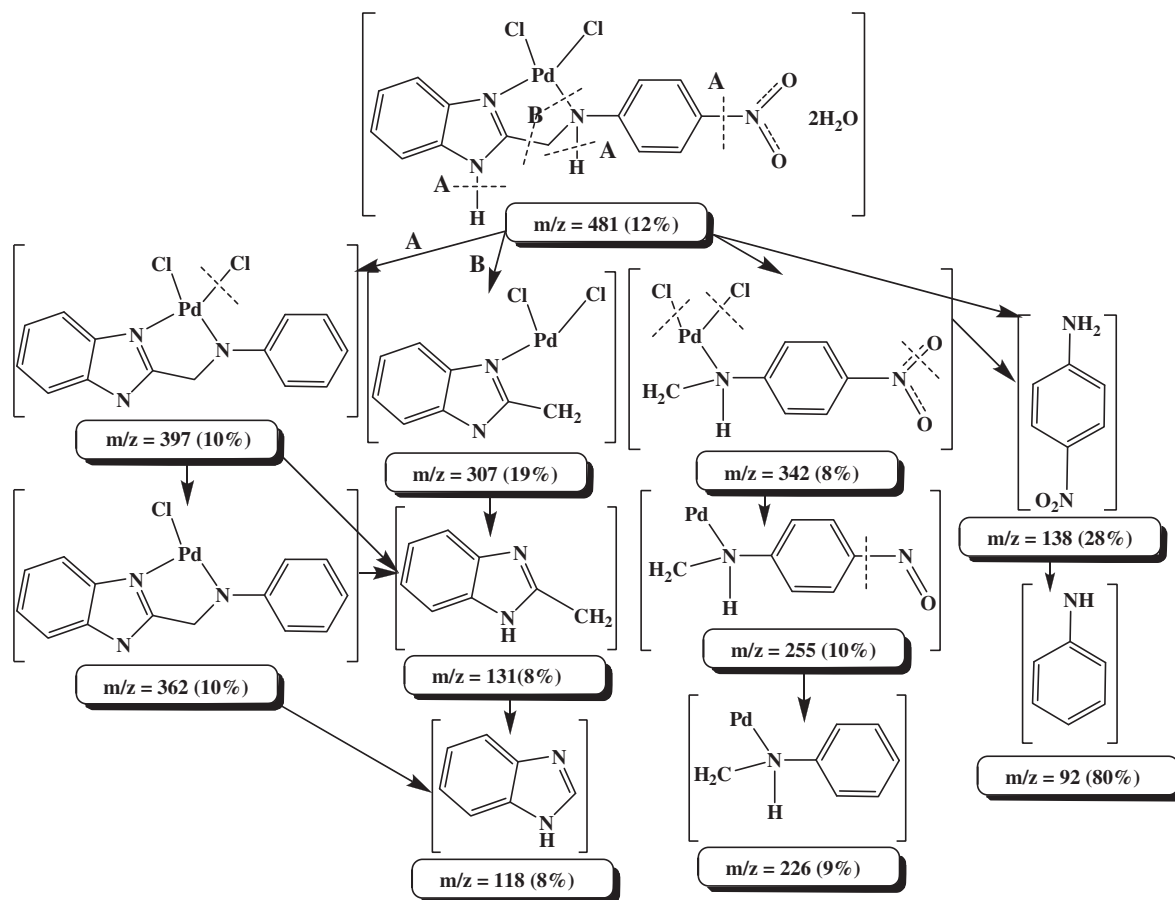
The Pt-L complex has a strong M^+ at m/z 534 owing to $[\text{PtLCl}_2]^+$ with three fragmentation routes. The first route is traced by a peak at m/z 450 owing to elimination of NO_2 , Cl, and ionizable protons from M^+ followed by the removal of imidazolic NH group and $2\text{C}_2\text{H}_2$ molecules from the benzimidazole ring to give a fragment at m/z 350. Thus, the participation of $\text{C}=\text{N}_{\text{py}}$ in the chelation introduces a weakness point through which the benzimidazole ring decomposes to imidazole moiety. The second route involves the loss of 2Cl and oxygen gas to provide a peak at m/z 431. The third route engages the loss of C_2H_2 from the benzimidazole ring to give a fragment at m/z 509.

3.4. Electronic absorption

3.4.1. Electronic absorption spectra in organic solvents

The electronic spectrum of L displayed five absorption bands in ethanol. The first and second bands at 206 and 230 nm may be assigned to the medium and low energy $\pi-\pi^*$ transitions within the phenyl rings of the aniline and benzimidazole moieties, respectively [32]. The shoulder at 240 nm and the bands at 273 and 280 nm may be assigned to $\pi-\pi^*$ transitions in the delocalized π -electron system and in the heteroatomic groups inside the benzimidazole molecule [33] as the $n-\pi^*$ transition is not observed in the benzimidazole compounds [34,35]. The bands at 273 and 280 nm appear doublet due to probable existence of a tautomeric structure [36] as supported by comparing our spectrum with that of 1-methyl-2-phenyl-benzimidazole [34], where this fine structure is lost. The longer wavelength band at 370 nm can be assigned to an intramolecular charge transfer interaction from the aromatic nucleus to the neighboring nitro acceptor center [32].

The absorption spectrum of L was observed in solvents of different polarity and of hydrogen bond formation tendency. The two bands at 274 and 280 nm in the cyclohexane (reference solvent) are slightly blue shifted in ethanol and 2-propanol (hydrogen-bonding solvents) suggests that the benzimidazole L is acting as a proton acceptor [37] at the pyridine-type nitrogen. However, the latter bands are red-shifted in DMF and DMSO (hydrogen bond acceptor solvents) due to an almost proton transfer from the solute molecules to these solvents. On the other hand, the CT band (370 nm) displayed a red shifted with increasing the solvent polarity, except for acetonitrile and dioxane, owing to a higher solvent stabilization of the excited state as the solvent polarity increases [32]. The values of the observed transition energies (E_{obs}) and oscillator strengths (f_{obs}) of all the bands in the electronic spectra of the benzimidazole L in different solvents were calculated [32] and



Scheme 1. Fragmentation pattern of Pd-L complex.

Table 1
Maximum wavelength (λ_{\max} , nm), wavenumber ($\bar{\nu}_{\max}$, cm^{-1}), molar absorptivity (ϵ_{\max} , $\text{L mol}^{-1} \text{cm}^{-1}$), π - π^* transition energy (E_{obs} , eV), and oscillator strength (f_{obs}), of benzimidazole L in different solvents.

Solvent	λ_{\max} (nm)	$\bar{\nu}_{\max} \times 10^4$ (cm^{-1})	$\epsilon_{\max} \times 10^4$	E_{obs} (eV)	f_{obs}	Solvent	λ_{\max} (nm)	$\bar{\nu}_{\max} \times 10^4$ (cm^{-1})	$\epsilon_{\max} \times 10^4$	E_{obs} (eV)	f_{obs}
Cyclohexane	248	4.03	0.96	5.01	0.09	Acetonitrile	232	4.31	1.07	5.35	0.23
	274	3.65	0.81	4.53	0.02		274	3.65	0.57	4.53	0.01
	280	3.57	0.80	4.43	0.01		280	3.57	0.61	4.43	0.01
	368	2.72	1.61	3.37	0.38		368	2.72	1.78	3.37	0.43
DMSO	275	3.64	0.14	4.52	0.01	Dioxane	235	4.26	1.57	5.28	0.28
	282	3.55	0.14	4.40	0.01		274	3.65	0.68	4.53	0.01
	387	2.58	1.94	3.21	0.35		281	3.56	0.71	4.42	0.01
DMF	263	3.80	1.04	4.72	0.03	2-Propanol	362	2.76	1.83	3.43	0.43
	274	3.65	0.50	4.53	0.01		235	4.26	0.67	5.28	0.11
	281	3.56	0.43	4.42	0.01		273	3.66	0.46	4.55	0.01
	382	2.62	1.96	3.25	0.37		280	3.57	0.52	4.43	0.01
Ethanol	206	4.85	1.27	6.03	0.25		370	2.70	1.73	3.36	0.41
	230	4.35	2.05	5.40	0.53						
	273	3.66	1.12	4.55	0.02						
	280	3.57	1.18	4.43	0.02						
	370	2.70	3.17	3.36	0.79						

tabulated in Table 1. Application of dielectric relation [32] to the band at 370 nm did not give a linear relation indicating that the spectral shifts are not governed solely by the dielectric effect of the solvents. However, the effects of solvent dipolarity/polarizability and hydrogen bonding on this band are interpreted by means of a linear solvation energy relationship [38], which indicates that the solvatochromism is mainly due to solvent dipolarity/polarizability.

3.4.2. Electronic absorption spectra in solutions of varying pH

The absorption spectra of 3×10^{-5} M solutions of compound L in 20% (v/v) ethanolic solutions of varying pH values were scanned in the UV-Vis. range. The CT band at 370 nm in ethanol is red shifted over the entire pH range from 376 nm (pH 2–4) to 386 nm at pH 12. This may be due to the lower percentage of ethanol in the buffering medium and the presence of water as the highly polar solvent. This is confirmed by observing the position

of this band at 387 nm in DMSO as previously discussed. With increasing $[H^+]$, a shoulder appears at 219 nm (pH 2) and vanishes with rising pH, corresponding to the deprotonation of pyridine-type nitrogen. The bands located at 273 and 280 nm in ethanol are blue shifted to 269 and 275 nm in the pH 2–4 (as found in ethanol and 2-propanol) owing to the protonation of N_{py} and NH_{sec} and these bands retain their positions between pH 6–12. The pH-absorbance changes [39] were utilized to calculate the acid dissociation constants. Four pK_a values were reported. The first one is 2.40 ± 0.02 corresponding to deprotonation of the protonated NH_{sec} . The pK_a value 5.21 ± 0.12 may be attributed to the ionization of the protonated N_{py} [35]. The third pK_a 7.52 ± 0.03 is accounted for the ionization of the NH_{sec} group, while the fourth pK_a 11.57 ± 0.02 is attributed to deprotonation of the NH_{Bz} group.

3.4.3. Electronic absorption spectra of complexes

The electronic spectra of 10^{-4} M of the studied complexes were scanned in DMF. The two bands between 270 and 280 nm ($35\,714\text{--}37\,000\text{ cm}^{-1}$) in the complexes are assigned to internal ligand transitions ($\pi\text{--}\pi^*$ in the benzimidazole ring). It is possible to calculate the value of Δ_1 from the first spin allowed d–d transition [40]. The first low energy spin allowed bands at $20\,408\text{ cm}^{-1}$ ($\Delta_1 = 22\,508\text{ cm}^{-1}$, $\log \epsilon_{max} = 4.12$) and $21\,231\text{ cm}^{-1}$ ($\Delta_1 = 23\,331\text{ cm}^{-1}$, $\log \epsilon_{max} = 4.06$) in Pd-L and Pt-L complexes, respectively, have been assigned to the transition $^1A_{1g} \rightarrow ^1A_{2g} (\nu_1)$. While, the band near $26,041\text{ cm}^{-1}$ in Pd-L ($\log \epsilon_{max} = 3.40$) is assigned to $^1A_{1g} \rightarrow ^1B_{1g} (\nu_2)$. The band at $27\,027\text{ cm}^{-1}$ ($\log \epsilon_{max} = 3.45$) in Pt-L complex is assigned to a combination of MLCT and $^1A_{1g} \rightarrow ^1E_g$ band (ν_3) [41]. Thus, the electronic spectra of these complexes are indicative of square planar geometry [41].

On the other hand, the benzimidazole L is considered to be excellent selective chromophoretic reagent for Pd(II) metal ion, this is indicated by the large difference in λ_{max} between the free ligand and the Pd-L complex (Fig. 2). It was found that, there is a difference of about 30 nm between the maximum wavelengths in the acidic and basic medium, and this may be due to conversion of dichloro palladium complex into dihydroxo one with increasing of pH.

3.5. Thermal analyses and kinetics studies

The TGA/DTA curves of Pd-L complex represent four decomposition steps. The first two endothermic stages at 72 and 240 °C are responsible for desorption of $3H_2O$ hydrated molecules. The third endothermic peak at 366 °C is assigned to elimination of $2H_2O$, Cl and one L molecule with a mass loss amounting to 63.20% (calcd.

63.36%). Desorption of these water molecules at relatively high temperature indicates the involvement of these molecules in hydrogen bond as confirmed from its mass spectrum, where a fragment at m/z 481 corresponding to $[PdClCl_2] \cdot 2H_2O$ was found. The final stage (620–1200 °C) brings the total mass loss up to 80.70% of the parent complex (80.19%) with a Pd as a final residue.

Discussing the simultaneous TGA/DTA curves constructed for Pt-L complex, one can observe two endothermic mass loss stages at 250 and 397 °C. The first stage is assigned to the exclusion of one chlorine atom with a mass loss 6.75% (calcd. 6.55%). The second step brings the total mass loss up to 60.06% of the parent complex (calcd. 61.24 %) with a Pt + C as a final residue [42]. Coats–Redfern [43] and Horowitz–Metzger methods [44] are used to calculate the thermodynamic parameters from TGA curves. It is found that the E^* and ΔG^* values increase on going from one thermal stage to another for a given complex, indicating that the rate of decomposition decreases in the same order. The positive ΔH^* values mean endothermic processes, while the negative ΔS^* values indicate that the complexes are formed spontaneously and are highly ordered in their activated states.

3.6. Theoretical calculations

3.6.1. Geometry optimization

Full geometry optimizations were performed at the DFT level of theory [13]. The optimized bond lengths of C=N and C–NH in the benzimidazole ring of compound L are 1.308 and 1.380 Å for B3LYP/6-311G (Supplementary material, Table S2). This discrepancy between C=N and C–NH, confirms that the hydrogen atom is fixed at one of the two nitrogen atoms through intermolecular hydrogen bond. These values coincide with those found from the optimization of 2-methylbenzimidazole and benzimidazole [45] under the same level of theory. The bicycle system of 2-methylbenzimidazole is planar [46] and the methyl group deviates from the planarity by 0.054° . Substitution of one hydrogen atom by 4-nitroaniline moiety shows essentially non-planar structure with dihedral angle $N_{15}\text{--}C_7\text{--}C_8\text{--}N_{17} = 126.6^\circ$ between the benzimidazole and aniline moieties. In addition, these latter bonds have a shorter distance than any amine compound, which is due to the participation of the lone electron pair of nitrogen atom in the resonance of the benzimidazole ring. The benzimidazole L shows accumulation of the negative charge density on the pyridine-type nitrogen, which is a very important structural feature related directly to the ability to bind the metal ions. Several calculated thermodynamic parameters are reported as (Supplementary material, Table S2).

The fully optimized geometries of cis-PdLCl₂ and cis-PtLCl₂ and numbering of atoms are shown in Fig. 3 and their selected geometric parameters are listed in Table 2. The coordination sphere around the metallic center in cis-PdLCl₂ and cis-PtLCl₂ complexes is made up of N_{py} , NH_{sec} and 2Cl completing the square planar geometry. The four donor atoms are coplanar, while the phenyl ring is bent out of the coordination plane by angle 88.861° and 157.428° for cis-PdLCl₂ and cis-PtLCl₂ complexes, respectively.

It was found that the Pd– NH_{sec} bond length is about 5.31% longer than the Pd– N_{py} bond distance [47]. It is seen that the optimized Pd– NH_{sec} and Pd– N_{py} bond lengths in cis-PdLCl₂ complex are slightly longer than the Pt– NH_3 bond distance in cis-platin by 0.17 and 0.06 Å, respectively, while the Pd–Cl bond lengths are longer than Pt–Cl by 0.05 and 0.03 Å for M–Cl22 and M–Cl23, respectively, owing to the trans-effect. Finally, the Pd– N_{py} (2.07 Å) and Pd– NH_{sec} (2.186 Å) bond lengths are in good agreement with that observed in some benzimidazole complexes [48]. The C13N11 and C14N21 bond lengths in cis-PdLCl₂ were increased upon the coordination of N_{py} , and NH_{sec} to the metal center as shown in Table 2. On the other hand, the Pt– NH_{sec} and Pt– N_{py}

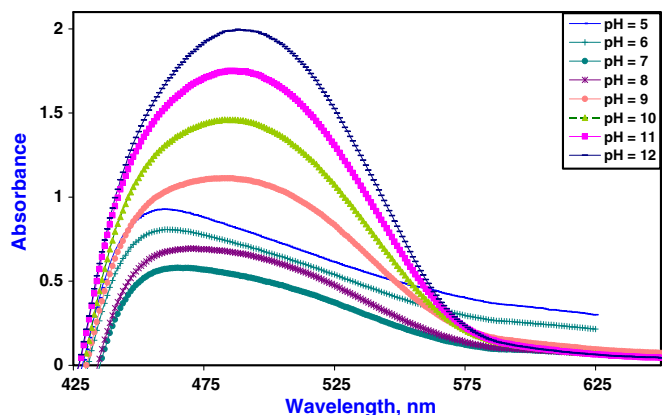


Fig. 2. Electronic absorption spectra of Pd-L complex in buffer solutions of varying pH.

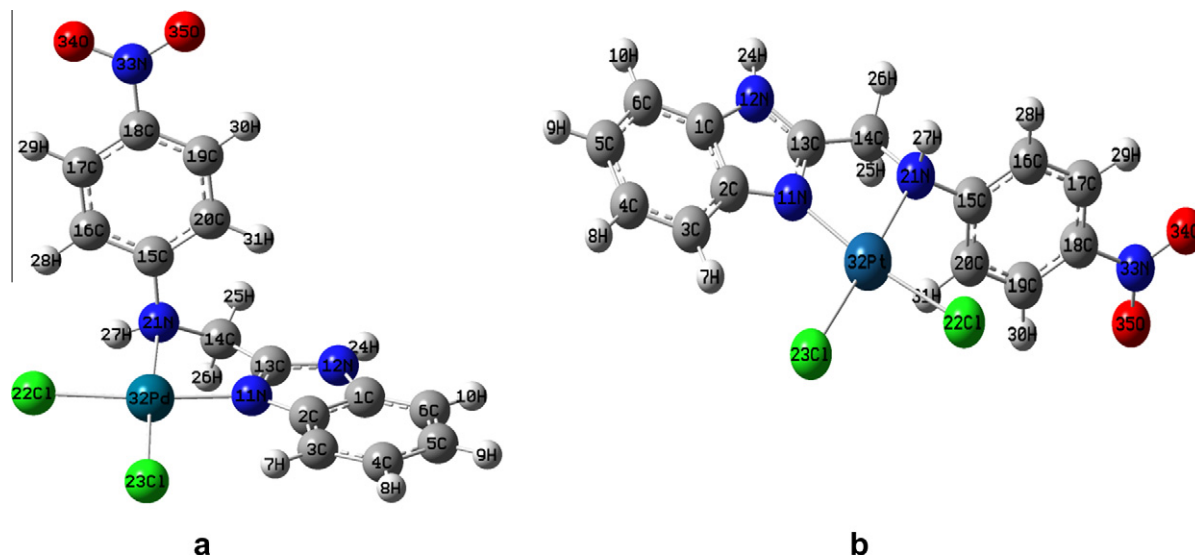


Fig. 3. Optimized structures of (a) cis-PdLCl₂ and (b) cis-PtLCl₂ complexes.

Table 2
Selected bond lengths (Å), angles (°) and charge for cis-PdLCl₂ and cis-PtLCl₂ complexes.

cis-PdLCl ₂				cis-PtLCl ₂							
Bond lengths (Å)		Bond angles (°)		Charge		Bond lengths (Å)		Bond angles (°)		Charge	
C1C2	1.425	C1C2C3	121.005	C1 = 0.151	C1C2	1.425	C1C2C3	120.752	C1 = 0.154		
C2C3	1.406	C2C3C4	116.969	C2 = 0.149	C2C3	1.407	C2C3C4	117.058	C2 = 0.149		
C3C4	1.402	C3C4C5	121.751	C3 = -0.187	C3C4	1.402	C3C4C5	121.854	C3 = -0.186		
C4C5	1.422	C4C5C6	121.668	C4 = -0.210	C4C5	1.421	C4C5C6	121.511	C4 = -0.211		
C5C6	1.404	C5C6C1	116.458	C5 = -0.195	C5C6	1.403	C5C6C1	116.497	C5 = -0.195		
C2N11	1.409	C6C1C2	122.148	C6 = -0.249	C2N11	1.415	C6C1C2	122.326	C6 = -0.250		
C1N12	1.411	C2N11C13	107.566	N11 = -0.561	C1N12	1.409	C2N11C13	107.346	N11 = -0.561		
C13N11	1.337	C1N12C13	107.675	N12 = -0.602	C13N11	1.338	C1N12C13	107.678	N12 = -0.597		
C13N12	1.378	N11C13N12	111.179	C13 = 0.468	C13N12	1.376	N11C13N12	111.350	C13 = 0.469		
C13C14	1.505	C13C14N21	108.629	C14 = -0.252	C13C14	1.497	C13C14N21	108.594	C14 = -0.242		
C14N21	1.502	C14N21C15	117.706	C15 = 0.193	C14N21	1.522	C14N21C15	111.854	C15 = 0.197		
C15N21	1.455	N21C15C16	118.266	C16 = -0.214	C15N21	1.471	N21C15C16	119.476	C16 = -0.226		
C15C16	1.413	C15C16C17	119.960	C17 = -0.167	C15C16	1.405	C15C16C17	119.859	C17 = -0.169		
C16C17	1.398	C16C17C18	119.041	C18 = 0.071	C16C17	1.403	C16C17C18	118.518	C18 = 0.079		
C17C18	1.407	C17C18C19	121.739	C19 = -0.169	C17C18	1.403	C17C18C19	122.173	C19 = -0.166		
C18C19	1.404	C18C19C20	118.989	C20 = -0.252	C18C19	1.407	C18C19C20	118.784	C20 = -0.217		
C19C20	1.401	C19C20C15	120.005	N21 = -0.693	C19C20	1.399	C19C20C15	119.652	N21 = -0.699		
C15C20	1.411	C20C15C16	120.259	Cl22 = -0.542	C15C20	1.407	C20C15C16	120.995	Cl22 = -0.514		
N11Pd	2.070	N11PdN21	80.555	Cl23 = -0.485	N11Pt	2.052	N11PtN21	81.0082	Cl23 = -0.481		
N21Pd	2.186	Cl22PdCl23	94.889	Pd = 0.685	N21Pt	2.155	Cl22PtCl23	90.7672	Pt = 0.618		
Cl22Pd	2.384	O34N33O35	123.828	N33 = 0.44352	Cl22Pt	2.400	O34N33O35	123.908	N33 = 0.445		
Cl23Pd	2.360			O34 = -0.36389	Cl23Pt	2.390			O34 = -0.367		
N33C18	1.474			O35 = -0.37392					O35 = -0.363		
N33O34	1.279										
N33O35	1.281										
<i>E</i> (a.u.)				-1066.689					-1059.102		
Zero-point <i>E</i> (kcal mol ⁻¹)				159.305					159.28091		
Rotational constants (GHz)				0.242, 0.125, 0.096					0.394, 0.093, 0.080		
Entropy (cal mol ⁻¹ K ⁻¹)											
Translational				44.161					44.706		
Rotational				35.954					35.944		
Vibrational				75.323					77.816		
Total dipole moment (D)				14.904					16.887		

bond lengths in cis-PtLCl₂ complex are shorter than the corresponding ones in the palladium complex by 0.02 and 0.03 Å, respectively.

The optimized N11–Pd–N21 (80.555°) is smaller than that found in cis-platin (NH₃–Pt–NH₃) by 6.445° and this can be interpreted in terms of CH₂ group, which connects the two coordination sites and prevent opening of this angle. The calculated Cl22–Pd–Cl23 (94.889°) angle is larger than the experimental one in

cis-platin molecule by 2.989° [49], since the intramolecular hydrogen bonding N21–H27···Cl22 (2.731 Å) opens up this angle. The optimized N11PtN21 is close to that found in cis-PdLCl₂ complex, while the Cl18PtC19 is slightly different from that exists in cis-platin by 2.99°. This indicates that there is a weak or almost no intramolecular hydrogen bonding as found in the cis-PdLCl₂ and this may be attributed to the significant difference in the bending angle of aniline ring as previously mentioned.

3.6.2. Natural bond orbital (NBO) analysis

The natural bond orbital (NBO) analysis of cis-PdLCl₂ complex was performed and could be used to estimate the delocalization of electron density between occupied Lewis-type orbitals and formally unoccupied non-Lewis NBOs (antibonding or Rydberg), which corresponds to a stabilizing donor–acceptor interaction [50]. Table 2 collects the natural charges on atoms. The largest negative charges are located on the two nitrogen atoms, N_{py} (−0.561e) and NH_{sec} (−0.693e). Thus, the bond lengths of PdN_{py} and PdNH_{sec} are different. According to the NBO, the electron configuration of Pd is: [core]5s^{0.35}4d^{8.94}5p^{0.02}5d^{0.01}6p^{0.01}. Thus, 36 core electrons, 9.29 valence electrons (on 5s and 4d atomic orbitals) and 0.036 Rydberg electrons (mainly on 5p, 5d and 6p orbitals) give the 45.315 electrons. This is consistent with the calculated natural charge on Pd atom (+0.685) in the palladium complex, which corresponds to the difference between 45.315e and the total number of electrons in the isolated Pd atom (46e). In addition, the two chlorine atoms (Cl22 and Cl23) have larger negative charge −0.542e and −0.485e, respectively. Thus, the positive atomic charge upon the Pd(II) was substantially reduced as a consequence of electron density donation from 2Cl, N_{py} and NH_{sec}.

Table 3 lists the calculated occupancies of natural orbitals. Three classes of NBOs are included, the Lewis-type (s and p bonding or lone pair) orbitals, the valence non-Lewis (acceptors, formally unfilled) orbitals and the Rydberg NBOs, which originate from orbitals outside the atomic valence shell. The calculated natural hybrids on atoms are also given in this Table 3. According to calculations, the palladium atom forms two sigma bonds with two chlorine atoms, while the two bonds between palladium and the nitrogen atoms can be described as donation of electron density from a lone pair (LP) orbital on each nitrogen atom to palladium molecular orbitals. As follows from Table 3, the σ(Pd–Cl22) bond is formed from an sp^{0.01}d^{1.09} hybrid on palladium atom (which is the mixture of 47.53% s, 0.47% p and 52.00% d atomic orbitals) and sp^{13.62} hybrid on the chlorine atom (93.16% p contribution). The results from NBO analysis show that the σ(Pd–Cl22) bond is strongly polarized towards the chlorine atom, with about 78.90% of electron density concentrated on the chlorine atom.

The strength of this interaction can be estimated by the second order perturbation theory.

Table 4 lists the selected values of the calculated second order interaction energy (E^2) between donor–acceptor orbitals in cis-PdLCl₂ complex. The strongest interactions are the electron donations from LP(1)N11 to the antibonding acceptor σ*(Pd–Cl22) orbitals, e.g. LP(1)N11 → σ*(Pd–Cl22). As shown in Table 3, the LP(1)N11 orbital has 69.39% p-character and is occupied by 1.728 electrons (this is consistent with a delocalization of electron density from the idealized occupancy of 2.0e). The donation of electron density from the coordination sites in the ligand to the Pd molecular orbitals has a clear correspondence to a chemical picture of the coordination bonds.

3.6.3. Frontier molecular orbitals

The frontier molecular orbitals play also an important role in the electric and optical properties, as well as in UV–Vis. spectra and chemical reactions [51]. Fig. 4 shows the distributions and energy levels of the HOMO–1, HOMO, LUMO and LUMO+1 orbitals computed at the B3LYP/LANL2DZ level for cis-PdLCl₂ complex. The values of the energy separation between the HOMO and LUMO are 3.02 and 3.32 eV for cis-PdLCl₂ and benzimidazole L, respectively.

3.7. Electrochemical studies

The redox behavior of the benzimidazole L and its Pd–L and Pt–L complexes were studied by cyclic voltammetry (CV) in DMF. The cyclic voltammogram of L displayed two reversible and quasi-reversible reduction peaks at $E_{1/2} = -1.42$ and -1.05 V. The first peak could be assigned to a four-electron reduction of nitro group generating the hydroxylamine derivative according to [52]: R-NO₂ + 4e[−] + 4H⁺ → R-NHOH + H₂O. The second cathodic peak assigned to the further reduction of the hydroxylamine to p-amino derivative. On the other hand, the irreversible anodic peak at 0.08 V is attributed to oxidization of the secondary amino group. In addition, the CV of the palladium complex exhibited two reversible reduction peaks (i_{pa}/i_{pc} is unity) at -1.10 and -0.60 V

Table 3
Occupancy of natural orbitals (NBOs) and hybrids calculated for cis-PdLCl₂ (selected).

Donor ^a Lewis-type NBOs (A–B)	Occupancy	Hybrid ^b	AO (%) ^c	Acceptor ^d nonLewis NBOs	NBOs
σ(C2–N11)	1.977	sp ^{1.93} (N11) sp ^{2.57} (C2)	s(34.18)p(65.82) s(27.97)p(72.03)	σ*(C2–N11)	0.033
σ(C13–N11)	1.978	sp ^{1.84} (N11) sp ^{2.12} (C13)	s(35.24)p(64.76) s(32.10)p(67.90)	σ*(C13–N11)	0.023
π(C13–N11)	1.899	sp(N11) sp ^{99.99} (C13)	s(0.01)p(99.99) s(0.01)p(99.99)	π*(C13–N11)	0.429
σ(C14–N21)	1.980	sp ^{2.52} (N21) sp ^{3.43} (C14)	s(28.41)p(71.59) s(22.56)p(77.44)	σ*(C14–N21)	0.022
σ(C15–N21)	1.985	Sp ^{1.95} (N21) sp ^{2.75} (C15)	s(33.12)p(66.88) s(33.78)p(66.13)	σ*(C15–N21)	0.038
σ(Pd–Cl22)	1.935	sp ^{0.01} d ^{1.09} (Pd) sp ^{13.62} (Cl22)	s(47.53)p(0.47)d(52.00) s(6.84)p(93.16)	σ*(Pd–Cl22)	0.324
σ(Pd–Cl23)	1.928	sp ^{0.01} d ^{1.03} (Pd) sp ^{15.68} (Cl23)	s(48.91)p(0.52)d(50.57) s(6.00)p(94.00)	σ*(Pd–Cl23)	0.268
σ(N21–H27)	1.980	sp ^{2.94} (N21)	s(25.39)p(74.61)		
LP(1)N11	1.728	sp ^{2.27}	s(30.61)p(69.39)	RY*(1)N11	0.008
LP(1)N21	1.713	sp ^{7.12}	s(12.31)p(87.69)	RY*(1)N21	0.007
LP(1)Cl22	1.991	sp ^{0.26}	s(79.52)p(20.48)	RY*(1)Cl22	0.0003
LP(1)Cl23	1.989	sp ^{0.54}	s(64.92)p(35.08)	RY*(1)Cl23	0.0004
LP(1)Pd	1.995	sp ^{0.21} d ^{99.99}	s(0.30)p(0.07)d(99.63)	RY*(1)Pd	0.017
LP(2)Pd	1.991	sp ^{0.08} d ^{99.99}	s(0.68)p(0.06)d(99.26)	RY*(2)Pd	0.003
LP(3)Pd	1.988	sp ^{0.03} d ^{64.23}	s(1.53)p(0.05)d(98.42)	RY*(3)Pd	0.002

^a LP(n)A is a valence lone pair orbital (n) on A atom.

^b Hybrid on A atom in the A–B bond or otherwise, as indicated.

^c Percentage contribution of atomic orbitals in NBO hybrid.

^d Starred label (*) denotes antibonding, and Ry corresponds to the Rydberg NBO orbital.

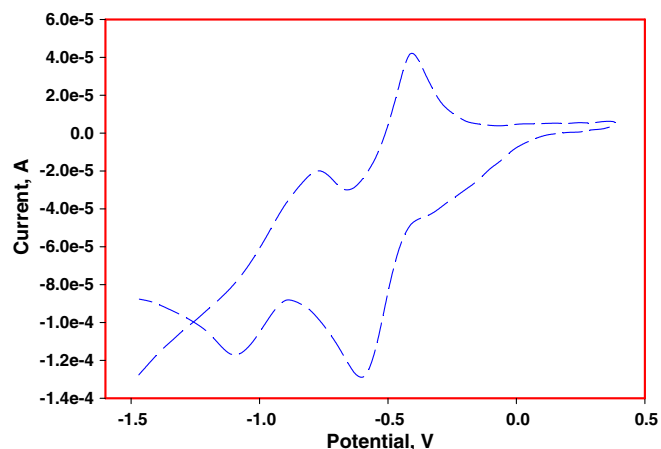
Table 4

Second-order interaction energy (E^2 , kcal/mol) between donor and acceptor orbitals in cis-PdCl₂ complex calculated at B3LYP/LANL2DZ level of theory (selected).

Donor → acceptor	E^2	Donor → acceptor	E^2
LP(1)N11 → $\sigma^*(\text{Pd}-\text{Cl}22)$	66.85	$\sigma(\text{N}11-\text{C}13) \rightarrow \sigma^*(\text{Pd}-\text{Cl}22)$	3.56
LP(1)N21 → $\sigma^*(\text{Pd}-\text{Cl}23)$	45.85	$\sigma(\text{N}21-\text{H}27) \rightarrow \sigma^*(\text{Pd}-\text{Cl}23)$	3.02
$\sigma(\text{Pd}-\text{Cl}23) \rightarrow \sigma^*(\text{Pd}-\text{Cl}22)$	14.09	$\sigma(\text{N}21-\text{C}14) \rightarrow \sigma^*(\text{Pd}-\text{Cl}23)$	1.72

corresponding to reduction of nitro group as shown in Fig. 5. The reduction process is shifted towards lower potential revealed an enhancement of the reduction process in the presence of palladium. The disappearance of anodic process indicated the participation of the secondary amino group in the complex formation. On the other hand, the platinum complex showed the first reduction process at -1.12 V.

It might be tempting now to correlate the values E_{red} derived from CV with HOMO–LUMO energy differences obtained from DFT calculations. The UV–Vis. absorption of a molecule corresponds indeed to excitation of an electron from the HOMO into the LUMO, whereas electro-oxidation corresponds only to the removal of an electron from the HOMO. A correlation might be possible if reduction of this molecule (i.e. donation of an electron into the LUMO) may be possible; in this case, the potential difference between oxidation and reduction potentials may be correlated with the HOMO–LUMO energy gap [53]. The potential difference between the reduction peaks ($\text{R}-\text{NO}_2 \rightarrow \text{R}-\text{NHOH}$) in the benzimidazole and that of its Pd-L complex is 0.32 V, which is in a good agreement with the shift associated the HOMO–LUMO gaps on going from the benzimidazole L to its palladium complex (0.30 eV). The DFT data have assigned that the LUMO of the Pd-L complex is constituted mainly by the nitro group of the ligand and thus the reduction is considered as electron accommodation at nitro dominated orbitals.

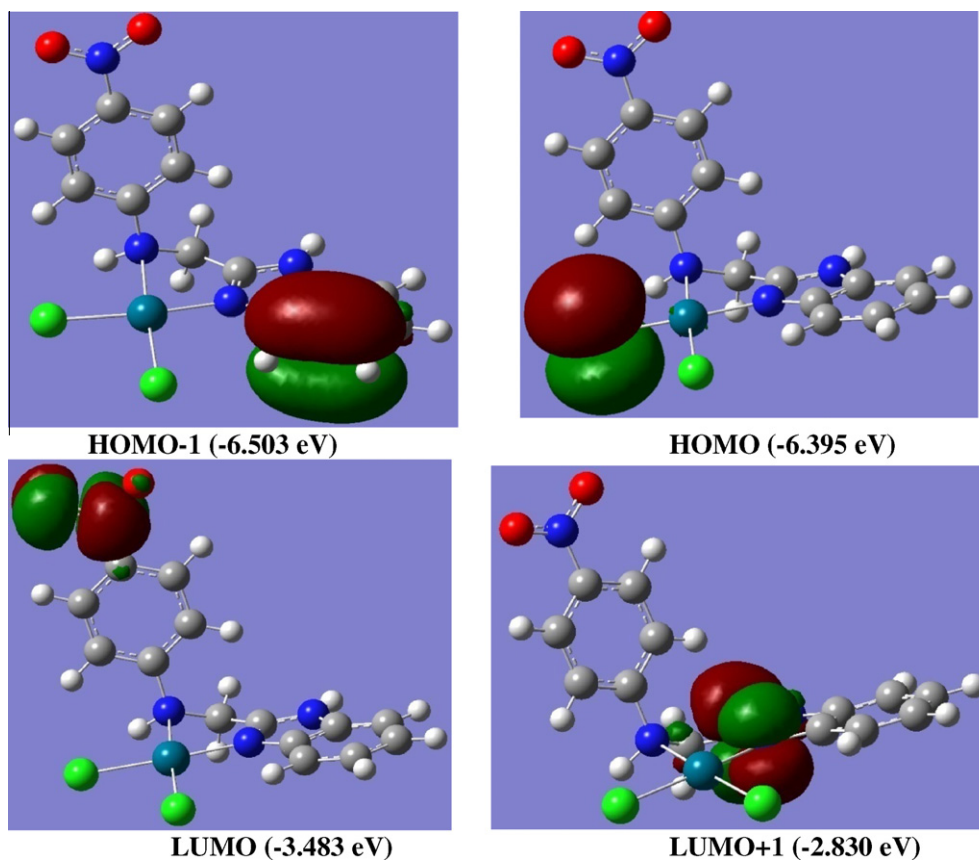
**Fig. 5.** Cyclic voltammogram of Pd-L complex.

In the present study, the molar conductance values of 10^{-3} M for Pd-L and Pt-L in DMF revealed low conductance values 14.16 and $20.81 \Omega^{-1} \text{cm}^2 \text{mole}^{-1}$, respectively, this may be taken as an evidence for the presence of chlorine atoms inside the coordination sphere of these complexes, indicating the non-electrolytic nature of these complexes.

3.8. Biological activity studies

3.8.1. Antimicrobial activity

The data showed that the ligand L and its complexes have the capacity of inhibiting the metabolic growth of the investigated

**Fig. 4.** Molecular orbital surfaces and energy levels of cis-PdCl₂ complex.

bacteria, *B. subtilis*, *S. aureus* and *S. faecalis* as Gram-positive bacteria and *P. aeruginosa*, *E. coli* and *N. gonorrhoeae* as Gram-negative bacteria, to different extents. The size of the inhibition zone depends upon the culture medium, incubation conditions, rate of diffusion and the concentration of the antibacterial agent (the activity increases as the concentration increases). In the present study, the benzimidazole L and its Pt-L complex are active against both types of the bacteria, which may indicate broad-spectrum properties. The remarkable activity of these compounds may be arising from the benzimidazole ring, which may play an important role in the antibacterial activity. The mode of action may involve the formation of a hydrogen bond through the tertiary nitrogen of the imidazole ring with the active centers of the cell constituents, resulting in interference with the normal cell process.

The Pd-L complex is only toxic against *E. coli* and *N. gonorrhoeae* as Gram-negative bacteria. The inhibitory activity of this complex is related to the cell wall structure of the bacteria. This is possible because the cell wall is essential to the survival of bacteria and some antibiotics are able to kill bacteria by inhibiting a step in the synthesis of peptidoglycan [54]. A possible explanation for the poor activity of these complexes with respect to their ligand may be attributed to their inability to chelate metals essential for the metabolism of microorganisms and/or to form hydrogen bonds with the active centers of cell structures, resulting in an interference with the normal cell cycle. Furthermore, the low activity of these complexes may be also due to their low lipophilicity, because of which penetration of the complex through the lipid membrane was decreased and hence, they could neither block nor inhibit the growth of the microorganism. Therefore, we confirm that the toxicity of the complexes can be related to the strengths of the M–L bond, in addition to other factors such as size of the cation, and receptor sites.

3.8.2. Antitumor activity

To evaluate the potential usefulness of palladium and platinum complexes synthesized as antitumor agents, three cell lines of different origin, *breast cancer* (MCF-7), *colon Carcinoma* (HCT) and *human hepatocellular Carcinoma* (Hep-G2) were treated. All the studied compounds showed activity against all the studied cell lines. On screening, it was found that Pd-L is more toxic than Pt-L against the studied cells at 100 μM . This happens because the ligand-exchange behavior of platinum compounds is quite slow, which gives them a high kinetic stability and results in ligand-exchange reactions of minutes to days, rather than microseconds to seconds for many other coordination compounds. In addition, another unusual phenomenon deals with the preferred ligands for platinum ions is that Pt(II) has a strong thermodynamic preference for binding to S-donor ligands and for this reason, one would predict that platinum compounds would perhaps never reach DNA, with many cellular platinumophiles (S-donor ligands, such as glutathione, methionine) as competing ligands in the cytosol [55]. These complexes show higher activity at 100 μM against Hep-G2 cells in comparable with cis-platin and nearly the same activity against the other cells.

4. Conclusion

Better approaches to the synthesis of the benzimidazole L and its complexes were developed. The comparisons of the DFT/B3LYP (6-311G(d,p) and LANL2DZ) calculations (vibrational and ^1H NMR) the benzimidazole L showed excellent agreement. The inclusion of solvation to the ^1H NMR calculations is necessary especially for acidic protons in order to obtain accurate values. The equilibrium geometries, harmonic frequencies, and FT-IR intensities of the metal complexes were determined and analyzed at DFT level of theory utilizing LANL2DZ basis set. NBO analysis re-

veals that the strong coordination bonds result from donation of electron density from a lone pair orbital on the nitrogen atoms to the acceptor metal molecular orbitals, e.g. (LP(1)N11 \rightarrow σ^* (Pd–Cl22)) and (LP(1)N21 \rightarrow σ^* (Pd–Cl23)). It was found that the studied compounds have the capacity of inhibiting the metabolic growth of the investigated bacteria to different extents. In addition, the complexes are toxic against three cell lines of different origin and represent an interesting class of new compounds from the viewpoint of their physicochemical and structural properties. Based on the results obtained from the physico-chemical techniques and theoretical calculations of the metal complexes, one can conclude that the studied ligand behaves as a neutral bidentate ligand coordinated to the metal ions via the pyridine-type nitrogen of the benzimidazole ring and secondary amino group. Thus, square planar geometry is suggested for the studied complexes, [PtLCl₂] and [PdLCl₂] \cdot 5H₂O.

Acknowledgments

We would like to extend our grateful thanks to Prof. Rifaat Hilal, Chemistry Department, Faculty of Science, Cairo University for allowing us to use his version of the GAUSSIAN98W package of programs.

Appendix A. Supplementary material

Supplementary data associated with this article can be found, in the online version, at doi:10.1016/j.ica.2011.04.036.

References

- [1] (a) I.H. Krakoff, in: M. Nicali (Ed.), "Platinum and Other Metal Coordination Compounds in Cancer Chemotherapy": Clinical Application of Platinum Complexes, Martinus Nijhoff, Boston, MA, 1988, p. 351; (b) E.R. Jamieson, S.J. Lippard, Chem. Rev. 99 (1999) 2467.
- [2] I. Kostova, Recent Patents Anti-Cancer Drug Discov. 1 (2006) 1.
- [3] (a) F. Gumus, G. Eren, L. Acik, A. Celebi, F. Ozturk, R. Iikci Sagkan, S. Gur, A. Ozkul, A. Elmali, Y. Elerman, J. Med. Chem. 52 (5) (2009) 1345; (b) M. Goekce, S. Utku, S. Guer, A. Oezkul, F. Gumus, Eur. J. Med. Chem. 40 (2) (2005) 135; (c) F. Gumus, O. Algul, G. Eren, H. Eroglu, N. Diril, S. Gur, A. Ozkul, Eur. J. Med. Chem. 38 (5) (2003) 473; (d) F. Gumus, A.B. Demirci, T. Oezden, H. Eroglu, N. Diril, Pharmazie 58 (5) (2003) 303; (e) F. Gumus, I. Pamuk, T. Oezden, S. Yildiz, N. Diril, E. Oksuzoglu, S. Gur, A. Ozkul, J. Inorg. Biochem. 94 (3) (2003) 255.
- [4] (a) V. Rajendiran, M. Murali, E. Suresh, S. Sinha, K. Somasundaram, M. Palaniandavar, Dalton Trans. (2008) 148; (b) J. Mann, A. Baron, Y. Opoku-Boahen, E. Johansson, G. Parkinson, L.R. Kelland, S. Neidle, J. Med. Chem. 44 (2001) 138.
- [5] J.B. Camden, US Patent 6077,862, 2002.
- [6] P.K. Naithani, V.K. Srivastava, A.K. Saxena, J.P. Barthwal, T.K. Gupta, K. Shanker, Indian J. Exp. Biol. 28 (1990) 1145.
- [7] N.M. Goudgaon, V. Dhondiba, A. Vijayalaxmi, Indian J. Heterocycl. Chem. 13 (2004) 271.
- [8] (a) E. Bouwmann, W.L. Driessen, J. Reedijk, Coord. Chem. Rev. 104 (1990) 143; (b) M.A. Puja, T.D. Bharamgouda, N.D. Sathyanarayana, Transition Met. Chem. 13 (1988) 423.
- [9] (a) Phillips, J. Chem. Soc. (1928) 2393; (b) H. Skolnik, J. Miller, A.R. Day, J. Am. Chem. Soc. 65 (1943) 1854.
- [10] A.D. Becke, J. Chem. Phys. 98 (1993) 5648.
- [11] C. Lee, W. Yang, R.G. Parr, Phys. Rev. B. 37 (1988) 785.
- [12] M.J. Frisch, G.W. Trucks, H.B. Schlegel, G.E. Scuseria, M.A. Robb, J.R. Cheeseman, V.G. Zakrzewski, J.A. Montgomery, R.E. Stratmann, J.C. Burant, S. Dapprich, J.M. Millam, A.D. Daniels, K.N. Kudin, M.C. Strain, O. Farkas, J. Tomasi, V. Barone, M. Cossi, R. Cammi, B. Mennucci, C. Pomelli, C. Adamo, S. Clifford, J. Ochterski, G.A. Petersson, P.Y. Ayala, Q. Cui, K. Morokuma, D.K. Malick, A.D. Rabuck, K. Raghavachari, J.B. Foresman, J. Cioslowski, J.V. Ortiz, A.G. Baboul, B.B. Stefanov, G. Liu, A. Liashenko, P. Piskorz, I. Komaromi, R. Gomperts, R.L. Martin, D.J. Fox, T. Keith, M.A. Al-Laham, C.Y. Peng, A. Nanayakkara, C. Gonzalez, M. Challacombe, P.M.W. Gill, B.G. Johnson, W. Chen, M.W. Wong, J.L. Andres, M. Head-Gordon, E.S. Replogle, J.A. Pople, GAUSSIAN 03 (Revision A.9), GAUSSIAN, Inc., Pittsburgh, 2003.
- [13] H.B. Schlegel, J. Comput. Chem. 3 (1982) 214.
- [14] A. Frisch, A.B. Nielson, A.J. Holder, GAUSSVIEW User Manual, GAUSSIAN Inc., Pittsburgh, PA, 2000.
- [15] R. Ditchfield, Chem. Phys. 76 (1972) 5688.

- [16] (a) D. Greenwood, *Antimicrobial Chemotherapy, Part II, Laboratory Aspects of Antimicrobial Therapy*, Bailliere, Tindall, London, 1983, p. 71;
(b) V. Lorian, *Antibiotics in Laboratory Medicine*, Williams and Wilkins, Baltimore, 1996.
- [17] National Committee for Clinical Laboratory Standards, *NCCLS Approval Standard Document M2-A7*, Vilanova, PA, 2000.
- [18] C.M. Lozano, O. Cox, M.M. Muir, J.D. Morales, J.L. Rodríguez-Cabáin, P.E. Vivas-Mejía, F.A. Gonzalez, *Inorg. Chim. Acta* 271 (1998) 137.
- [19] (a) P. Skehan, R. Smreng, D. Scudiero, A. Monks, J. McMahon, D. Vistica, J.T. Warren, H. Bokesch, S. Kenney, M.R. Boyd, *J. Nat. Cancer Inst.* 82 (1990) 107;
(b) A. Monks, D. Scudiero, P. Skehan, K. Paull, D. Vistica, C. Hose, J. Langley, P. Cronise, A. Viagro-Wolff, M. Gra-Goodrich, *J. Nat. Cancer Inst.* 83 (1991) 757.
- [20] (a) G. Rauhut, P. Pulay, *J. Phys. Chem.* 99 (1995) 3093;
(b) J.A. Pople, H.B. Schlegel, R. Krishnan, J.S. Defrees, J.S. Binkley, M.J. Frisch, R.A. Whiteside, *Int. J. Quant. Chem.: Quant. Chem. Symp.* 15 (1981) 269.
- [21] (a) M.W. Ellzy, J.O. Jensen, H.F. Hameka, J.G. Kay, D. Zeroka, *Spectrochim. Acta* 57A (2001) 2417;
(b) J.O. Jensen, A. Banerjee, C.N. Merrow, D. Zeroka, J.M. Lochner, *J. Mol. Struct.: Theochem.* 531 (2000) 323;
(c) J.O. Jensen, D. Zeroka, *J. Mol. Struct.: Theochem.* 487 (1999) 267.
- [22] O. Sala, N.S. Goncalves, L.K. Noda, *J. Mol. Struct.* 411 (2001) 565.
- [23] K. Hofmann, *Imidazole and Its Derivatives*, Interscience Publishers, New York, 1953.
- [24] S. Satyanarayana, K.R. Nagasundara, *Synth. React. Inorg. Met.-Org. Chem.* 34 (5) (2004) 883.
- [25] R.W. Hay, T. Clifford, P.L. Foot, *Polyhedron* 17 (20) (1998) 3575.
- [26] (a) S. Mohan, N. Sundaraganesan, *Spectrochim. Acta (A)* 47 (1991) 1111;
(b) N. Sundaraganesan, S. Ilakiamani, P. Subramani, B. Dominic Joshua, *Spectrochim. Acta Part A* 67 (2007) 628.
- [27] (a) N.M. Agathabay, M. Tulu, M. Somer, D. Hacıu, A. Yilmaz, *Struct. Chem.* 19 (2008) 21;
(b) F.S. Miranda, F.G. Menezes, J. Vicente, A.J. Bortoluzzi, C. Zucco, A. Neves, N.S. Gonçalves, *J. Mol. Struct.* 938 (2009) 1.
- [28] K. Nakamoto, "Infrared and Raman Spectra of Inorganic and Coordination Compounds", Part B: Applications in Coordination, Organometallic, and Bioinorganic Chemistry, sixth ed., John Wiley and sons Inc., New Jersey, 2009.
- [29] W. Nawrocka, B. Sztuba, M.W. Kowalaka, H. Liszkiewicz, *Farmaco* 59 (2004) 83.
- [30] J.D. Crane, R. Hughes, E. Sinn, *Inorg. Chim. Acta* 237 (1995) 181.
- [31] (a) E. Bednarek, J.C. Dobrowolski, K. Dobrosz-Teperek, L. Kozerski, W. Lewandowski, A.P. Mazurek, *J. Mol. Struct.* 554 (2000) 233;
(b) F.S. Miranda, F.G. Menezes, J. Vicente, A.J. Bortoluzzi, C.Z. Ademir-Neves, N.S. Gonçalves, *J. Mol. Struct.* 938 (2009) 1.
- [32] (a) R.M. Issa, A.A. Hassanein, I.M. El-Mehasseb, R.I. Abed, El-Wadoud, *Spectrochim. Acta Part A* 65 (2006) 206;
(b) R.M. Issa, K.Y. El-baradie, N.A. El-Wakiel, *Spectrochim. Acta Part A* 60 (2004) 2883.
- [33] G.G. Araya-Hernandez, R.G.E. Morales, *J. Photochem. Photobiol. A: Chem.* 177 (2006) 125.
- [34] M. Krishnamurthy, P. Phaniraj, S.K. Dogra, *J. Chem. Soc., Perkin Trans. II* (1986) 1917 (and the references therein).
- [35] A.K. Mishra, S.K. Dogra, *Bull. Chem. Soc. Jpn.* 58 (1985) 3587;
J. Photochem. 31 (1985) 333;
Indian J. Phys., Sect. B 54 (1984) 480;
Spectrochim. Acta. Part A 39 (1983) 609.
- [36] R.M. Issa, S.A. El-Daly, N.A. El-Wakiel, *Spectrochim. Acta Part A* 59 (2003) 723.
- [37] P.N. Preston, *Benzimidazoles and Congeneric Tricyclic Compounds*, Part I, Wiley, New York, 1981. p. 64.
- [38] S.N. Azizi, M.J. Chaichi, M. Yousefi, *Spectrochim. Acta Part A* 73 (2009) 101.
- [39] I.M. Issa, R.M. Issa, M.S. El-Ezaby, Y.Z. Ahemed, *Z. Physik. Chem.* 242 (1969) 169. 250 (1972) 161.
- [40] O.E. Offiong, S. Martelli, *Transition Met. Chem.* 22 (1997) 263.
- [41] (a) A.B.P. Lever, *Inorganic Electronic Spectroscopy*, second ed., Elsevier, Amsterdam, 1982. p. 544;
(b) D.X. West, M.S. Lockwood, A. Liberta, X. Chen, R.D. Willet, *Transition Met. Chem.* 18 (1993) 221.
- [42] (a) I. Lakomska, M. Barwiolek, E. Szlyk, *Transition Met. Chem.* 32 (2007) 70;
(b) A. Bakalova, H. Varbanov, R. Buyukliev, G. Momekov, D. Ivanov, *J. Thermal Anal. Calorim.* 95 (2009) 241.
- [43] A.W. Coats, J.P. Redfern, *Nature* 201 (1964) 68.
- [44] H.H. Horowitz, G. Metzger, *Anal. Chem.* 85 (1963) 1464.
- [45] R.I. Castillo, S.P.H. Rivera, *J. Mol. Struct.* 917 (2009) 158.
- [46] R.I. Castillo, L.A.R. Montalvo, S.P.H. Rivera, *J. Mol. Struct.* 877 (2008) 10.
- [47] D.N. Neogi, P. Das, A.N. Biswas, P. Bandyopadhyay, *Polyhedron* 25 (2006) 2149.
- [48] (a) R.W. Hay, T. Clifford, P. Lightfoot, *Polyhedron* 17 (20) (1998) 3575;
(b) X. Jing-Yuan, G. Wen, L. Ling, Y. Shi-Ping, C. Peng, L. Dai-Zheng, J. Zong-Hui, *J. Mol. Struct.* 644 (2003) 2327.
- [49] R. Wysokiński, D. Michalska, *J. Comput. Chem.* 22 (9) (2001) 901.
- [50] A.E. Reed, L.A. Curtius, F. Weinhold, *Chem. Rev.* 88 (1988) 899.
- [51] I. Fleming, *Frontier Orbitals and Organic Chemical Reactions*, Wiley, London, 1976.
- [52] A. Álvarez-Lueje, C. Zapata-Urzuá, S. Brain-Isasi, M. Pérez-Ortiz, L. Barros, H. Pessoa-Mahana, M.J. Kogan, *Talanta* 79 (2009) 687.
- [53] M. Al-Anber, B. Milde, W. Alhalasah, H. Lang, R. Holze, *Electrochim. Acta* 53 (2008) 6038.
- [54] A.L. Koch, *Clin. Microbiol. Rev.* 16 (2003) 673.
- [55] M. Pérez-Cabré, G. Cervantes, V. Moreno, M.J. Prieto, J.M. Pérez, M. Font-Bardia, X. Solans, *J. Inorg. Biochem.* 98 (2004) 510.